Inverse problems

Reconstruction of viscoelastic tissue properties from MR elastography-type measurements

Reconstruction des propriétés viscoélastiques des tissus utilisant des mesures d'élastographie par résonance magnétique

Huina Yuan, Bojan B. Guzina *

Department of Civil Engineering, University of Minnesota, Minneapolis, MN 55455, USA

ABSTRACT

This study is concerned with an optimization-based approach to the identification of "background" viscoelastic properties of soft tissues from magnetic resonance (MR) elastography-type measurements. In this approach, the triaxial tissue displacements, captured by the MR scanner over a suitable subdomain that is free of major heterogeneities, are split into (i) a boundary subset that is used to formulate the forward (Dirichlet) problem, and (ii) an internal subset, employed as "the data" for the inverse (material characterization) problem. For an elevated performance of the minimization scheme, material sensitivities of the featured cost functional are computed semi-analytically via a boundary-integral formulation, resulting in alternative "direct" and adjoint-field sensitivity formulas. The numerical results, obtained assuming input parameters that are relevant to MR elastography, indicate that the proposed approach may provide an effective means for comprehensive multi-frequency characterization of the "background" viscoelasticity of soft tissues.

© 2010 Académie des sciences. Published by Elsevier Masson SAS. All rights reserved.

RÉSUMÉ

L'objet de cette étude est l'identification des propriétés viscoélastiques « ambiantes » d'un tissu mou par un processus d'optimisation reposant sur des mesures fournies par élastographie par résonance magnétique (IRM). Dans cette approche, les déplacements triaxiaux au sein du tissu (mesurés par le scanner IRM) dans un sous domaine d'intérêt, sans hétérogénéités majeures, sont séparés en (i) données de frontière utilisées pour formuler le problème (Dirichlet) direct, et (ii) mesures internes constituant les « données » pour le problème inverse (de caractérisation des matériaux). Pour une performance accrue de l'algorithme de minimisation, les sensibilités matériaux de la fonction coût considérée sont calculées semi-analytiquement par une formulation d'intégrales de frontières aboutissant à des formules de sensibilités reposant sur des champs « direct » et adjoint. Les résultats numériques, obtenus en utilisant des paramètres pertinents pour l'élastographie par résonance magnétique, montrent que l'approche proposée peut constituer un moyen efficace pour une caractérisation multi-fréquentielle exhaustive de la viscoélasticité « ambiante » des tissus mous.

© 2010 Académie des sciences. Published by Elsevier Masson SAS. All rights reserved.

* Corresponding author.

1. Introduction

Magnetic resonance (MR) elastography is a novel imaging technique for the spatial reconstruction of effective viscoelastic properties in soft tissues [1–3]. Since its inception [1], the technique has been applied to breast tumor [4–6], liver tumor [7,8] and brain degeneration imaging [9] with promising results. The basic idea of the MR elastography is to vibrate the tissue in a steady-state fashion (at frequencies in the 0.01–1 kHz range) inside the scanner, and to capture the induced 3D motion, i.e. wave patterns in the tissue via suitable sequencing of the MR scans. With such kinematic information the viscoelastic tissue properties can, at a given control point, be estimated by numerically approximating (e.g. via finite differences) and algebraically manipulating the *local* equations of motion [3,4]. Frequently enhanced by the introduction of a numerical curl operator [6] to filter the effect of compressional waves, such local "inversion" of the governing differential equations has gained popularity due to its simplicity and low computational cost. Despite its advantages, however, this approach is hampered by simplifying assumptions such as material isotropy and homogeneity [3,4], and the necessity to numerically evaluate the second- or even third-order [6] spatial derivatives of the observed displacement field. In terms of the MR applications, the latter requirement translates into (i) elevated sensitivity to measurement uncertainties, and (ii) strict limitations on the excitation frequencies, i.e. wavelengths that can be handled by the given spatial resolution of an MR scanner (often on the order of a millimeter).

An alternative technique for the geometric reconstruction and material characterization of inner heterogeneities using mechanical waves is the so-called method of topological sensitivity [10–13], which identifies obstacles via the distribution of the namesake indicator function. In particular the topological sensitivity, which quantifies the perturbation of a given cost functional due to the nucleation of an infinitesimal defect in the reference ("defect-free") solid [14,15], is used as an effective obstacle indicator through an assembly of sampling points where it attains extreme negative values. This technique, which is computationally effective as it entails the calculation of only two (visco-) elastodynamic states for the reference solid, however *assumes* the knowledge of the constitutive properties of the latter. In the context of medical imaging, such "prior" information on the reference, i.e. background solid is unfortunately patient-specific and must be obtained on a case-by-case basis.

To help resolve the problem, this investigation establishes a systematic, minimization-based methodology for estimating the isotropic viscoelastic properties of a background (i.e. healthy) soft tissue from MR elastography measurements. This is accomplished by considering a sample subdomain, Ω, of the region tested (identified to be lesion-free on the basis of the "raw" MR images), and formulating an inverse problem where the motion measurements over $\partial\Omega$ are interpreted as the Dirichlet excitation used to "illuminate" the subdomain, whereas their companions taken strictly inside Ω are used as *the data*. In this setting, the minimization of the assumed (e.g. least-squares) misfit functional is facilitated by obtaining the formulas for its *material sensitivities* in a boundary-integral equation (BIE) setting that makes use of the adjoint-field approach and material-parameter sensitivities of the visco-elastodynamic fundamental solution [16]. Numerical results indicate that the proposed methodology may provide an effective means for estimating the (background) viscoelastic properties of soft tissues over a range of excitation frequencies, including those associated with shorter wavelengths where the local inversion approach [3,4,6] may not be effective. The latter feature may especially be useful in establishing the basis for "broad-band", high-resolution MR elastography that is yet to be developed.

2. Problem formulation

In the MR elastography experiment, time-harmonic excitation is applied to the surface of a tissue, and the tissue's displacement response is monitored over a uniform *3D grid* of internal points commensurate with the spatial resolution of an MR device [4]. To identify the tissue's "background" viscoelastic properties, the idea is to select a cubic subdomain Ω (free of major heterogeneities) whose closure $\overline{\Omega} = \Omega \cup \Gamma$, $\Gamma = \partial\Omega$ contains $(N+2)^3$ measurement grid points, and to solve the inverse problem for a homogeneous solid cube whose Dirichlet boundary conditions (taken as the excitation, i.e. input to the direct problem) are computed by interpolating $(6N^2 + 12N + 8)$ triaxial displacement measurements taken over Γ. In what follows, the featured inverse problem is formulated in a continuum setting where the viscoelastic material properties of a finite body are sought on the basis of the prescribed boundary excitation and observed internal motion, monitored over a set of interior points. Assuming further the boundary excitation to be time-harmonic [6], the material characterization problem reduces, by virtue of the correspondence principle [17], to the reconstruction of the solid's complex-valued and frequency-dependent "elastic" parameters, one frequency at a time.

2.1. Direct and inverse problem

Consider the boundary value problem for a finite, homogeneous, viscoelastic body Ω that is vibrated, at frequency ω, via Dirichlet boundary excitation $\boldsymbol{\psi}$ prescribed over $\Gamma = \partial\Omega$. In the isotropic material setting assumed hereon, the body is characterized by its mass density ρ, complex-valued shear modulus $\mu = \mu(\omega)$, and complex-valued Poisson's ratio $\nu = \nu(\omega)$. On denoting by $\boldsymbol{u}$ the displacement field induced in the solid, the featured direct problem can accordingly be written as

E-mail addresses: yuanx039@umn.edu (H. Yuan), guzina@wave.ce.umn.edu (B.B. Guzina).

$$\mathcal{L}\boldsymbol{u} = \boldsymbol{0}, \quad \boldsymbol{\xi} \in \Omega$$
$$\boldsymbol{u} = \boldsymbol{\psi}, \quad \boldsymbol{\xi} \in \Gamma \tag{1}$$

where

$$\mathcal{L}(\cdot) = \nabla \cdot \big(\boldsymbol{C} : \nabla(\cdot)\big) + \rho\omega^2(\cdot) \tag{2}$$

is the Navier operator, and

$$\boldsymbol{C} = \frac{2\mu(1+\nu)}{3(1-2\nu)}\boldsymbol{I}_2 \otimes \boldsymbol{I}_2 + 2\mu\left(\boldsymbol{I}_4 - \frac{1}{3}\boldsymbol{I}_2 \otimes \boldsymbol{I}_2\right)$$

is the isotropic viscoelasticity tensor.

To characterize the body in terms of its viscoelastic and mass density properties, the experimental displacement field, hereon denoted by $\boldsymbol{u}^{\text{obs}}$, is monitored over a prescribed grid of measurement points uniformly distributed over $\Omega \cup \Gamma$. Consistent with earlier discussion, this data set is *split* as $\boldsymbol{u}^{\text{obs}} = \boldsymbol{u}_\Gamma^{\text{obs}} \cup \boldsymbol{u}_\Omega^{\text{obs}}$, where the boundary observations $\boldsymbol{\psi} = \boldsymbol{u}_\Gamma^{\text{obs}}$ are used to construct the Dirichlet excitation for (1), while the internal observations, $\boldsymbol{u}_\Omega^{\text{obs}}$, are used as "the data". As a result, the sought vector of material properties

$$\boldsymbol{\alpha} = (\mu, \nu, \rho) \tag{3}$$

can be conveniently estimated by minimizing the cost functional

$$\mathcal{J}(\boldsymbol{\alpha}) = \int\limits_\Omega \varphi\big(\boldsymbol{u}(\boldsymbol{x}), \boldsymbol{u}^{\text{obs}}(\boldsymbol{x}), \boldsymbol{x}\big)\, \mathrm{d}\Omega_x \tag{4}$$

where the distance function φ, which quantifies the misfit between the trial displacement field $\boldsymbol{u}$ (computed for given $\boldsymbol{\psi}$ and trial $\boldsymbol{\alpha}$) and its observed counterpart $\boldsymbol{u}^{\text{obs}}$, is assumed to be differentiable with respect to its first argument. In the case of the least-squares cost functional and spatially-discrete observations that are relevant to this study, one further has

$$\varphi\big(\boldsymbol{u}, \boldsymbol{u}^{\text{obs}}, \boldsymbol{x}\big) = \frac{1}{2}\sum_{m=1}^M \big|\boldsymbol{u} - \boldsymbol{u}^{\text{obs}}\big|^2 \delta\big(\boldsymbol{x} - \boldsymbol{x}^m\big), \quad \boldsymbol{x}^m \in \Omega \tag{5}$$

where $\boldsymbol{x}^m$ signify the set of $M = N^3$ internal observation points. Given a moderate size of the parametric space (3), $\mathcal{J}$ can be effectively minimized via gradient-based optimization [18] where the key ingredient is an efficient and accurate evaluation of the cost functional sensitivities.

3. Material sensitivities

On employing the chain rule, the "material" sensitivities of a generic cost functional (4) with respect to the real and imaginary parts of the entries of $\boldsymbol{\alpha}$ can be computed as

$$\mathcal{J}_{k,\text{r}}'(\boldsymbol{\alpha}) \equiv \frac{\partial\mathcal{J}}{\partial\alpha_{k\text{r}}} = \text{Re}\left\{\int\limits_\Omega \varphi_{,\boldsymbol{u}}\big(\boldsymbol{u}, \boldsymbol{u}^{\text{obs}}, \boldsymbol{x}\big) \cdot \boldsymbol{u}_k'\, \mathrm{d}\Omega\right\}, \quad \alpha_{k\text{r}} = \text{Re}(\alpha_k)$$
$$\mathcal{J}_{k,\text{i}}'(\boldsymbol{\alpha}) \equiv \frac{\partial\mathcal{J}}{\partial\alpha_{k\text{i}}} = -\text{Im}\left\{\int\limits_\Omega \varphi_{,\boldsymbol{u}}\big(\boldsymbol{u}, \boldsymbol{u}^{\text{obs}}, \boldsymbol{x}\big) \cdot \boldsymbol{u}_k'\, \mathrm{d}\Omega\right\}, \quad \alpha_{k\text{i}} = \text{Im}(\alpha_k),\ k = 1, 2, 3 \tag{6}$$

where $\mathcal{J}_{3,\text{i}}' \equiv 0$ for the problem of interest (the mass density is real-valued), and

$$\varphi_{,\boldsymbol{u}} = \frac{\partial\varphi}{\partial(\text{Re}(\boldsymbol{u}))} - \mathrm{i}\frac{\partial\varphi}{\partial(\text{Im}(\boldsymbol{u}))}, \qquad \boldsymbol{u}_k' = \frac{\partial\boldsymbol{u}}{\partial\alpha_k}, \quad k = 1, 2, 3 \tag{7}$$

3.1. Direct approach

For an effective computation of the trial displacement field $\boldsymbol{u}$ and its material sensitivities $\boldsymbol{u}_k'$ ($k = 1, 2, 3$) in a homogeneous body Ω, one may conveniently employ the boundary-integral equation (BIE) formulation as in [19,20]. To this end, let $\boldsymbol{n}$ be a reference unit normal, and let $\mathbb{U}(\boldsymbol{\xi}, \boldsymbol{x})$ and $\mathbb{T}(\boldsymbol{\xi}, \boldsymbol{x}) = \boldsymbol{n} \cdot \boldsymbol{C} : \nabla_\xi\mathbb{U}$ denote respectively the displacement and traction (visco-elastodynamic) Green's tensors [13] for an infinite solid $\mathbb{R}^3$ with complex-valued constitutive parameters μ and ν, and mass density ρ. Here the Cartesian components of $\mathbb{U}(\boldsymbol{\xi}, \boldsymbol{x})$ and $\mathbb{T}(\boldsymbol{\xi}, \boldsymbol{x})$ are arranged such that $\mathbb{U} \cdot \boldsymbol{e}_j$ and $\mathbb{T} \cdot \boldsymbol{e}_j$ signify respectively the displacement and traction vectors at $\boldsymbol{\xi} \in \Omega$ due to a unit time-harmonic point force acting at $\boldsymbol{x} \in \Omega$ in the jth coordinate direction specified via unit vector $\boldsymbol{e}_j$, $j = 1, 2, 3$. With such definitions, the direct problem (1) can be reformulated in terms of the boundary-integral equation

$$\mathcal{H}[\boldsymbol{\psi}](\boldsymbol{x}) - \mathcal{G}[\boldsymbol{t}](\boldsymbol{x}) = \boldsymbol{0}, \quad \boldsymbol{x} \in \Gamma \tag{8}$$

where $\boldsymbol{t} = \boldsymbol{n} \cdot \boldsymbol{C} : \nabla\boldsymbol{u}$ denotes the surface traction on Γ ($\boldsymbol{n}$ is oriented toward the exterior of Ω), and the featured boundary-integral operators are defined as

$$\mathcal{H}[\boldsymbol{u}](\boldsymbol{x}) = \int_{\Gamma} \boldsymbol{u}(\boldsymbol{\xi}) \cdot \mathbb{T}(\boldsymbol{\xi}, \boldsymbol{x}) \, \mathrm{d}S_{\xi}, \qquad \mathcal{G}[\boldsymbol{t}](\boldsymbol{x}) = \int_{\Gamma} \boldsymbol{t}(\boldsymbol{\xi}) \cdot \mathbb{U}(\boldsymbol{\xi}, \boldsymbol{x}) \, \mathrm{d}S_{\xi} \tag{9}$$

On solving (8) for $\boldsymbol{t}$, the interior displacement field $\boldsymbol{u}$ can be computed by way of integral representation

$$\boldsymbol{u}(\boldsymbol{x}) = \mathcal{G}[\boldsymbol{t}](\boldsymbol{x}) - \mathcal{H}[\boldsymbol{\psi}](\boldsymbol{x}), \quad \boldsymbol{x} \in \Omega \tag{10}$$

By differentiating (10) with respect to α_k, one finds the material sensitivities $\boldsymbol{u}'_k$ to be computable as

$$\boldsymbol{u}'_k(\boldsymbol{x}) = \mathcal{G}[\boldsymbol{t}'_k](\boldsymbol{x}) + \mathcal{G}'_k[\boldsymbol{t}](\boldsymbol{x}) - \mathcal{H}'_k[\boldsymbol{\psi}](\boldsymbol{x}), \quad \boldsymbol{x} \in \Omega, \ k = 1, 2, 3 \tag{11}$$

where $\boldsymbol{t}'_k = \partial\boldsymbol{t}/\partial\alpha_k$, and

$$\mathcal{H}'_k[\boldsymbol{u}](\boldsymbol{x}) = \int_{\Gamma} \boldsymbol{u}(\boldsymbol{\xi}) \cdot \frac{\partial\mathbb{T}}{\partial\alpha_k}(\boldsymbol{\xi}, \boldsymbol{x}) \, \mathrm{d}S_{\xi}, \qquad \mathcal{G}'_k[\boldsymbol{t}](\boldsymbol{x}) = \int_{\Gamma} \boldsymbol{t}(\boldsymbol{\xi}) \cdot \frac{\partial\mathbb{U}}{\partial\alpha_k}(\boldsymbol{\xi}, \boldsymbol{x}) \, \mathrm{d}S_{\xi} \tag{12}$$

noting that the explicit expressions for $\partial\mathbb{U}/\partial\alpha_k$ and $\partial\mathbb{T}/\partial\alpha_k$ can be found in [16]. To compute $\boldsymbol{t}'_k$, on the other hand, one may differentiate the governing boundary-integral equation (8) with respect to α_k which yields

$$\mathcal{G}[\boldsymbol{t}'_k](\boldsymbol{x}) = \mathcal{H}'_k[\boldsymbol{\psi}](\boldsymbol{x}) - \mathcal{G}'_k[\boldsymbol{t}](\boldsymbol{x}), \quad \boldsymbol{x} \in \Gamma, \ k = 1, 2, 3 \tag{13}$$

In the context of (8) and (13), it is noted that operators $\mathcal{G}$ and $\mathcal{G}'_k$ are only weakly singular, whereas $\mathcal{H}$ and $\mathcal{H}'_k$ are both Cauchy singular [16]. The latter impediment can, however, be rectified via the usual decomposition procedure [19,20] which employs the fact that the leading singular behavior of $\mathbb{T}$ (and consequently that of $\mathbb{T}'_k$) is given by the corresponding elastostatic solution ($\omega = 0$). Once $\boldsymbol{t}'_k$ over Γ is computed from (13), the substitution of (11) into (6) yields the sought material sensitivities as

$$\begin{bmatrix} \mathcal{J}'_{k,\mathrm{r}} \\ \mathcal{J}'_{k,\mathrm{i}} \end{bmatrix}(\boldsymbol{\alpha}) = \begin{bmatrix} \mathrm{Re} \\ -\mathrm{Im} \end{bmatrix} \left\{ \int_{\Omega} \varphi_{,\boldsymbol{u}}(\boldsymbol{u}, \boldsymbol{u}^{\mathrm{obs}}, \boldsymbol{x}) \cdot \left(\mathcal{G}[\boldsymbol{t}'_k](\boldsymbol{x}) + \mathcal{G}'_k[\boldsymbol{t}](x) - \mathcal{H}'_k[\boldsymbol{\psi}](\boldsymbol{x}) \right) \mathrm{d}\Omega_x \right\}, \quad k = 1, 2, 3 \tag{14}$$

where $\boldsymbol{t}$ on Γ is computed by solving (8). In general, formulas (14) entail volume integration of surface integrals (9) and (12) which, owing to the singularity of the featured Green's functions, may require specialized numerical treatment for quadrature points $\boldsymbol{x}$ that are close to Γ. In situations involving discrete motion measurements as in (5), however, this difficulty is normally circumvented due to the fact that the distance between the observation points $\boldsymbol{x}^m$ ($m = 1, 2, \ldots, M$) and Γ is bounded from below by the spacing of the measurement grid.

3.2. Adjoint-field approach

To establish the adjoint-field counterpart of (14), one may recall that $\boldsymbol{u}$ is governed by (1) and let $\dot{\boldsymbol{u}}$ denote the so-called adjoint field, defined in the usual way as a solution of the boundary value problem

$$\begin{aligned} \mathcal{L}\dot{\boldsymbol{u}} + \varphi_{,\boldsymbol{u}} &= \boldsymbol{0}, \quad \boldsymbol{\xi} \in \Omega \\ \dot{\boldsymbol{u}} &= \boldsymbol{0}, \quad \boldsymbol{\xi} \in \Gamma \end{aligned} \tag{15}$$

where $\mathcal{L}$ is given by (2), and $\varphi_{,\boldsymbol{u}} = \partial\varphi/\partial\boldsymbol{u}(\boldsymbol{u}, \boldsymbol{u}^{\mathrm{obs}}, \boldsymbol{\xi})$ is computed in the sense of (7).

Domain-integral formula. The computation of $\mathcal{J}'_{k,\mathrm{r}}$ and $\mathcal{J}'_{k,\mathrm{i}}$ can next be facilitated by differentiating (1) with respect to α_k, which yields

$$\begin{aligned} \mathcal{L}\boldsymbol{u}'_k + \mathcal{L}'_k\boldsymbol{u} &= \boldsymbol{0}, \quad \boldsymbol{\xi} \in \Omega \\ \boldsymbol{u}'_k &= \boldsymbol{0}, \quad \boldsymbol{\xi} \in \Gamma, \quad k = 1, 2, 3 \end{aligned} \tag{16}$$

Here $\boldsymbol{u}$ solves (1);

$$\mathcal{L}'_k(\cdot) = \nabla \cdot \left(\boldsymbol{C}_{,\alpha_k} : \nabla(\cdot) \right) + \delta_{k3}\omega^2(\cdot) \tag{17}$$

δ stands for the Kronecker delta, and $\boldsymbol{u}'_k \equiv \partial\boldsymbol{u}/\partial\alpha_k$ is the sought sensitivity field generated by an effective body force $\mathcal{L}'_k\boldsymbol{u}$. On exercising the Graffi's reciprocity identity in terms of visco-elastodynamic states $\dot{\boldsymbol{u}}$ and $\boldsymbol{u}'_k$, one finds that

$$\int_{\Omega} \left\{ \varphi_{,\boldsymbol{u}} \cdot \boldsymbol{u}'_k - \mathcal{L}'_k\boldsymbol{u} \cdot \dot{\boldsymbol{u}} \right\} \mathrm{d}\Omega_{\xi} = \int_{\Gamma} \left\{ \boldsymbol{\tau}'_k \cdot \dot{\boldsymbol{u}} - \dot{\boldsymbol{t}} \cdot \boldsymbol{u}'_k \right\} \mathrm{d}S_{\xi} \tag{18}$$

where $\dot{\boldsymbol{t}} = \boldsymbol{n} \cdot \boldsymbol{C} : \nabla \dot{\boldsymbol{u}}$ and $\boldsymbol{\tau}'_k = \boldsymbol{n} \cdot \boldsymbol{C} : \nabla \boldsymbol{u}'_k$ (note that $\boldsymbol{\tau}'_k \neq \boldsymbol{t}'_k$). By virtue of the homogeneous boundary conditions $\dot{\boldsymbol{u}} = \boldsymbol{0}$ and $\boldsymbol{u}'_k = \boldsymbol{0}$ on Γ, (18) can be reduced as

$$\int_{\Omega} \varphi_{,\boldsymbol{u}} \cdot \boldsymbol{u}'_k \, \mathrm{d}\Omega_\xi = \int_{\Omega} \mathcal{L}'_k \boldsymbol{u} \cdot \dot{\boldsymbol{u}} \, \mathrm{d}\Omega_\xi \tag{19}$$

which, in light of (6), yields the adjoint-field material sensitivity formula

$$\begin{bmatrix} \mathcal{J}'_{k,\mathrm{r}} \\ \mathcal{J}'_{k,\mathrm{i}} \end{bmatrix} (\boldsymbol{\alpha}) = \begin{bmatrix} \mathrm{Re} \\ -\mathrm{Im} \end{bmatrix} \left\{ \int_{\Omega} \mathcal{L}'_k \boldsymbol{u} \cdot \dot{\boldsymbol{u}} \, \mathrm{d}\Omega_\xi \right\}, \quad k = 1, 2, 3 \tag{20}$$

as the volume integral of a bilinear form involving the trial field $\boldsymbol{u}$ and the adjoint field $\dot{\boldsymbol{u}}$. Here it is useful to note that (20), which notably requires the second-order derivatives of $\boldsymbol{u}$, is amenable to a variety of computational treatments including finite element, finite difference, and BIE techniques. In terms of the latter class of methods, however, the computation of material sensitivities following (20) is further complicated by the frequency-dependent density of quadrature that may be necessary to accurately evaluate the featured domain integral.

Boundary-integral formula. To provide a surface-integral alternative to (14) and (20), one may apply the Graffi's reciprocity identity to $\boldsymbol{u}$ and $\dot{\boldsymbol{u}}$ which, on exercising the respective boundary conditions in (1) and (15), yields

$$\int_{\Omega} \varphi_{,\boldsymbol{u}} \cdot \boldsymbol{u} \, \mathrm{d}\Omega_\xi = -\int_{\Gamma} \dot{\boldsymbol{t}} \cdot \boldsymbol{\psi} \, \mathrm{d}S_\xi \tag{21}$$

On differentiating (21) with respect to α_k while considering the adjoint body-force excitation $\varphi_{,\boldsymbol{u}}$ as given, i.e. *invariant* under the perturbation of material properties, one finds that

$$\int_{\Omega} \varphi_{,\boldsymbol{u}} \cdot \boldsymbol{u}'_k \, \mathrm{d}\Omega_\xi = -\int_{\Gamma} \dot{\boldsymbol{t}}'_k \cdot \boldsymbol{\psi} \, \mathrm{d}S_\xi \tag{22}$$

where $\dot{\boldsymbol{t}}'_k = \partial \dot{\boldsymbol{t}} / \partial \alpha_k$. By virtue of (6), this result yields the surface integral representation of material sensitivities as

$$\begin{bmatrix} \mathcal{J}'_{k,\mathrm{r}} \\ \mathcal{J}'_{k,\mathrm{i}} \end{bmatrix} (\boldsymbol{\alpha}) = \begin{bmatrix} -\mathrm{Re} \\ \mathrm{Im} \end{bmatrix} \left\{ \int_{\Gamma} \dot{\boldsymbol{t}}'_k \cdot \boldsymbol{\psi} \, \mathrm{d}S_\xi \right\}, \quad k = 1, 2, 3 \tag{23}$$

To compute $\dot{\boldsymbol{t}}'_k$ within the framework of the BIE methods, one may formulate (15) as a boundary-integral equation

$$\mathcal{G}[\dot{\boldsymbol{t}}](\boldsymbol{x}) = -\int_{\Omega} \varphi_{,\boldsymbol{u}}(\boldsymbol{\xi}) \cdot \mathbb{U}(\boldsymbol{\xi}, \boldsymbol{x}) \, \mathrm{d}\Omega_\xi, \quad \boldsymbol{x} \in \Gamma \tag{24}$$

and differentiate (24) with respect to α_k, to obtain

$$\mathcal{G}[\dot{\boldsymbol{t}}'_k](\boldsymbol{x}) = -\mathcal{G}'_k[\dot{\boldsymbol{t}}](\boldsymbol{x}) - \int_{\Omega} \varphi_{,\boldsymbol{u}}(\boldsymbol{\xi}) \cdot \frac{\partial \mathbb{U}}{\partial \alpha_k}(\boldsymbol{\xi}, \boldsymbol{x}) \, \mathrm{d}\Omega_\xi, \quad \boldsymbol{x} \in \Gamma \tag{25}$$

Here it is noted that, in the BIE setting, the solution of (24) is required for the computation of *both* (20) and (23). In this light representation (23) requires the solution of an additional BIE, namely (25), which still entails domain integration. Nonetheless, (23) is deemed to surpass (20) in terms of BIE computations in that: (i) it is free of the second-order derivatives of $\boldsymbol{u}$ which may be cumbersome to compute, and (ii) for discrete observations as in (5), the volume integral on the right-hand side of (25) can be computed *exactly* as a weighted summation of M Green's function sensitivities regardless of the excitation frequency.

4. Computational treatment and minimization

In what follows, the material identification scheme based on the gradient-based minimization of (4) and "direct" material sensitivity formula (14) is implemented by way of the BIE framework as in [20].

4.1. Evaluation of material sensitivities

With reference to (8) and (13), the computation of $\mathcal{J}'_k$ ($k = 1, 2, 3$) entails the solution of *four* boundary-integral equations over Γ, where (13) must be evaluated (and solved) for each k. Written in terms of the "primary" tractions $\boldsymbol{t}$ over Γ and their material-sensitivity companions $\boldsymbol{t}'_k$ as the problem unknowns, these BIE's can be discretized and represented via respective algebraic systems as

Primary: $\qquad\qquad GT = HU$

Material sensitivity: $\quad GT'_k = H'_k U - G'_k T, \quad k = 1, 2, 3$ $\qquad\qquad\qquad\qquad$ (26)

Here vectors U and T contain the nodal approximations of the primary displacement and traction fields, $u = \psi$ and t, on Γ; the coefficient matrices H and G approximate the respective boundary-integral operators $\mathcal{H}$ and $\mathcal{G}$ in (8); vector T'_k refers to t'_k, while H'_k and G'_k are the matrix discretizations of $\mathcal{H}'_k$ and $\mathcal{G}'_k$ in (13). In terms of the computational effort required to solve (26), it is noted that the coefficient matrix, G, is *the same* for all four discretized systems. As a result, the solution of the remaining three algebraic systems can be obtained at significantly reduced cost once the first system has been solved. Assuming hereon a discrete set of internal observation points and the least-squares distance functional as in (5), the cost functional $\mathcal{J}$ and its sensitivities $\mathcal{J}'_k$ can, with U, T and T'_k in place, be computed as

$$\mathcal{J}(\boldsymbol{\alpha}) = \frac{1}{2} \sum_{m=1}^{M} \left| u(x^m) - u^{\mathrm{obs}}(x^m) \right|^2, \qquad u(x^m) = \mathcal{G}[t](x^m) - \mathcal{H}[\psi](x^m)$$

$$\begin{bmatrix} \mathcal{J}'_{k,\mathrm{r}} \\ \mathcal{J}'_{k,\mathrm{i}} \end{bmatrix}(\boldsymbol{\alpha}) = \begin{bmatrix} \mathrm{Re} \\ -\mathrm{Im} \end{bmatrix} \left\{ \sum_{m=1}^{M} \overline{(u(x^m) - u^{\mathrm{obs}}(x^m))} \cdot \left(\mathcal{G}[t'_k](x^m) + \mathcal{G}'_k[t](x^m) - \mathcal{H}'_k[\psi](x^m) \right) \right\}$$

where the expression for $u(x^m)$ is understood in a discretized sense and $k = 1, 2, 3$.

4.2. Minimization

As examined earlier, the goal of this study is the material characterization of a homogeneous viscoelastic body via nonlinear minimization of the cost functional (4). To maintain the physical significance of a solution, however, the arguments of $\mathcal{J}$, i.e. the components of $\boldsymbol{\alpha}$ must be subject to suitable inequality constraints. In the context of isotropic viscoelasticity, it can be shown that besides $\rho > 0$, one has $\mathrm{Re}(\mu) > 0$ and $\mathrm{Im}(\mu) \geqslant 0$ as the necessary conditions for thermomechanical stability [17]. In terms of the complex-valued Poisson's ratio where the constraints are more complicated, on the other hand, it is found [21] that $0 \leqslant \mathrm{Re}(\nu) < 0.5$ and $\mathrm{Im}(\nu) \leqslant 0$ represent meaningful restrictions on most viscoelastic materials. Since the majority of constrained minimization algorithms provide only *soft* bounds that can be violated during the minimization process [18], it is next essential to *restate* the vector of material properties $\boldsymbol{\alpha}$ as to enforce most of the above constraints. To this end, one may introduce an auxiliary vector $\boldsymbol{\beta} = (\beta_1, \beta_2, \beta_3, \beta_4, \beta_5) \in \mathbb{R}^5$ where

$$\beta_1 = \log(\alpha_{1\mathrm{r}}), \qquad \beta_2 = \log(\alpha_{1\mathrm{i}}), \qquad \beta_3 = \log(0.5 - \alpha_{2\mathrm{r}}), \qquad \beta_4 = \log(-\alpha_{2\mathrm{i}}), \qquad \beta_5 = \log(\alpha_3) \qquad (27)$$

so that inequalities $\mathrm{Re}(\mu) > 0$, $\mathrm{Im}(\mu) > 0$, $\mathrm{Re}(\nu) < 0.5$, $\mathrm{Im}(\nu) < 0$ and $\rho > 0$ are identically met. On the basis of this result, the material sensitivity of $\mathcal{J}$ with respect to the components of $\boldsymbol{\beta}$ can be computed in terms of $\partial \mathcal{J} / \partial \alpha_k$ as

$$\frac{\partial \mathcal{J}}{\partial \beta_1} = \frac{\partial \mathcal{J}}{\partial \alpha_{1\mathrm{r}}} \alpha_{1\mathrm{r}}, \qquad \frac{\partial \mathcal{J}}{\partial \beta_2} = \frac{\partial \mathcal{J}}{\partial \alpha_{1\mathrm{i}}} \alpha_{1\mathrm{i}}, \qquad \frac{\partial \mathcal{J}}{\partial \beta_3} = \frac{\partial \mathcal{J}}{\partial \alpha_{2\mathrm{r}}} (\alpha_{2\mathrm{r}} - 0.5), \qquad \frac{\partial \mathcal{J}}{\partial \beta_4} = \frac{\partial \mathcal{J}}{\partial \alpha_{2\mathrm{i}}} \alpha_{2\mathrm{i}}, \qquad \frac{\partial \mathcal{J}}{\partial \beta_5} = \frac{\partial \mathcal{J}}{\partial \alpha_3} \alpha_3 \qquad (28)$$

In light of (27) and (28), the minimization problem is next posed in a constrained fashion as

$$\min_{\beta} \mathcal{J}(\boldsymbol{\beta}), \qquad C_i(\boldsymbol{\beta}) \geqslant 0, \ \forall i \in \mathcal{I} \qquad\qquad\qquad\qquad (29)$$

where the *soft* inequality constraints C_i ($\mathcal{I}$ being a set of integers) reflect any relevant restrictions on the material properties that are not enforced via (27). By way of slack variables, the constrained optimization problem (29) can be further reduced to the unconstrained minimization of an augmented-Lagrangian cost functional [18] defined as

$$L(\boldsymbol{\beta}, \lambda^m, \gamma_m) \equiv \mathcal{J}(\boldsymbol{\beta}) + \sum_{i \in \mathcal{I}} \Phi(C_i(\boldsymbol{\beta}), \lambda_i^m, \gamma_m)$$

$$\Phi(C, \lambda, \gamma) = \begin{cases} -\lambda C + C^2 / 2\gamma, & C \leqslant \gamma\lambda \\ -\gamma\lambda^2 / 2, & C > \gamma\lambda \end{cases} \qquad\qquad\qquad\qquad (30)$$

where m is the iteration number, λ^m is the vector of Lagrange multipliers, and γ^m is the penalty parameter. For each iteration m, the minimization is carried out using the BFGS quasi-Newton method [18] and an inexact line search based on the strong Wolfe conditions [22].

4.3. Interpolation of Dirichlet data over Γ

A salient assumption behind the computation of $\mathcal{J}$ and its material sensitivities is that the observed Dirichlet data, $\psi = u_\Gamma^{\mathrm{obs}}$, are available *continuously* over Γ which allows one to formulate the underpinning boundary value problems in terms of the primary field u, adjoint field $\dot{u}$, and their sensitivities. In terms of (26), this hypothesis allows the vector of prescribed boundary displacements, U, to be constructed by sampling ψ at nodal coordinates of the featured boundary element mesh.
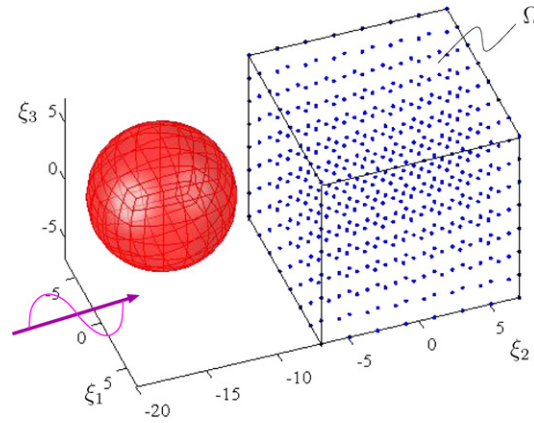
Fig. 1. Testing configuration for an infinite viscoelastic solid illuminated by shear plane wave: ball-shaped heterogeneity (left) and homogeneous cubical subdomain $\overline{\Omega} = \Omega \cup \Gamma$ (right) containing the 3D grid of measurement points.

In the context of *spatially-discrete* observations inherent to MR elastography [3,4], this hypothesis is unfortunately not met (see also (5)). In situations involving the cubic geometry of Ω such as those of interest in this study, however, the above impediment can be rectified by computing the entries of $\boldsymbol{U}$ via two-dimensional (2D) cubic spline interpolation of the grid values

$$\boldsymbol{\psi}^\ell = \boldsymbol{u}_\Gamma^{\mathrm{obs}}(\boldsymbol{x}^\ell), \quad \boldsymbol{x}^\ell \in \Gamma, \ \ell = 1, 2, \ldots, 6N^2 + 12N + 8$$

separately over each face of the cube, whose closure $\Omega \cup \Gamma$ contains $(N+2)^3$ triaxial measurement points as examined earlier.

5. Results

To examine the performance of the material identification approach, the foregoing methodology is employed to reconstruct the complex shear modulus of a viscoelastic solid (over a range of frequencies) assuming prior knowledge of its Poisson's ratio and mass density. With reference to Fig. 1, the host, i.e. background domain is taken as infinite viscoelastic solid, $\mathbb{R}^3$, perturbed by a stiff (ball-shaped) elastic inclusion to simulate the presence of material heterogeneities. In this setting, the solid is illuminated by an incident plane wave, with the triaxial displacement response measured over a uniform 3D grid of $(N+2)^3 = 8^3$ observations contained by the closure, $\Omega \cup \Gamma$, of a *homogeneous* cubical subdomain Ω that is used as the basis for material characterization. In what follows, the synthetic observations are generated using a viscoelastodynamic boundary element code [20] employing 216 quadratic (eight-node) elements over the surface of the sphere; the surface of the reference cubical domain, Γ, is discretized using 294 quadratic elements; and the minimization of $\mathcal{J}$ is effected assuming the least-squares distance function (5). For clarity it is emphasized that *neither* the information about the geometry of the host domain, its heterogeneities, *nor* the applied excitation are made available to the reconstruction scheme.

Motivated by the data from MR elastography studies [4,6], the Poisson's ratio and mass density of the background solid are taken as $\nu = 0.49$ and $\rho = 1050$ kg/m^3, while the measurement grid of 8^3 points ($N = 6$) is assumed to be uniformly distributed over the cubical volume $\overline{\Omega} = \{\boldsymbol{\xi}: |\xi_j| < 7$ mm, $j = 1, 2, 3\}$ with the nearest-neighbor separation of 2 mm. The "true" complex shear modulus of the background viscoelastic medium is taken as that of the *standard linear solid* [17], namely

$$\mu^{\mathrm{true}}(\omega) = \frac{\mu_s + (\mu_s + \mu_d)\mathrm{i}\omega\tau_r}{1 + \mathrm{i}\omega\tau_r} \tag{31}$$

where $\mu_s = 10$ kPa is the static shear modulus, $\mu_s + \mu_d = \lim_{\omega \to \infty} \mu = 20$ kPa is the "high-frequency" shear modulus, and $\tau_r = 0.0016$ s denotes the relaxation time. The Poisson's ratio and mass density of the ball-shaped inclusion are taken respectively as $\nu_b = 0.49$ and $\rho_b = 1550$ kg/m^3.

With reference to Table 1, the complex shear modulus of the background solid is reconstructed at four excitation frequencies ranging from 50 to 200 Hz. As a point of reference the MR elastography experiments in [6], that feature the same density of the testing grid, were performed at 65 Hz. As can be seen from the list, the direction and polarization of the incident (shear) plane wave, as well as the location, size and shear modulus μ_b of the spherical heterogeneity were *altered* from one excitation frequency to another to reflect the variation of wave patterns in a finite host domain (e.g. soft-tissue organ) with increasing rate of excitation. As examined earlier, the information in Table 1 was not furnished to (nor required by) the reconstruction scheme.

Table 1
Parameters of the illuminating plane wave and ball-shaped inclusion at sample testing frequencies.

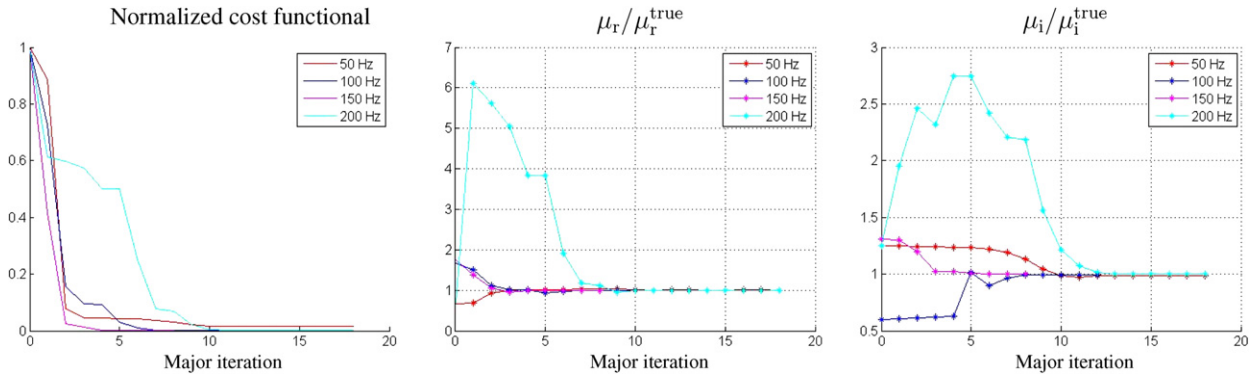| f [Hz]	Incidence	Polarization	Centroid [mm]	Diameter [mm]	μ_b [kPa]
50	$\frac{1}{\sqrt{2}}(1,1,0)$	$\frac{1}{\sqrt{5}}(-2,2,-1)$	$(-17,1.5,-1)$	15	$50+2i$
100	$(0,1,0)$	$\frac{1}{\sqrt{2}}(-1,0,-1)$	$(-2,-15,1)$	10	$60+4i$
150	$\frac{1}{\sqrt{5}}(1,0,2)$	$\frac{1}{5}(4,\sqrt{5},-2)$	$(2,-15,-5)$	10	$60+4i$
200	$\frac{1}{3}(1,2,2)$	$\frac{1}{3}(-2,2,1)$	$(2,-15,-5)$	10	$60+5i$

Fig. 2. Convergence of the reconstructed shear modulus, $\mu(\omega)$ at $\omega = 2\pi \times \{50, 100, 150, 200\}$ rad/s, of the background solid in terms of $\mu_r = \mathrm{Re}(\mu)$ and $\mu_i = \mathrm{Im}(\mu)$.

Table 2
Optimization results.

f [Hz]	μ^{true} [kPa]	λ [mm]	μ^{init} [kPa]	μ^{opt} [kPa]	$\mu^{\mathrm{opt}}_{\mathrm{noise}}$ [kPa]
50	$(12.0, 4.0)$	68	$(8.0, 5.0)$	$(12.0, 4.0)$	$(12.3, 3.2)$
100	$(15.0, 5.0)$	38	$(25.0, 3.0)$	$(14.9, 5.0)$	$(15.1, 5.0)$
150	$(17.0, 4.6)$	27	$(30.0, 6.0)$	$(17.0, 4.6)$	$(16.6, 4.6)$
200	$(18.0, 4.0)$	21	$(10.0, 5.0)$	$(18.0, 4.0)$	$(18.0, 4.0)$

The convergence of the optimization procedure at all four frequencies is illustrated, in terms of the real and imaginary parts of the reconstructed shear modulus, in Fig. 2. As can be seen from the display, the scheme converges to the global minimum after roughly 10–15 major iterations for the configurations examined. For completeness the "true" shear modulus μ^{true}, the wavelength λ of the illuminating shear waves, the initial "guess" μ^{init}, and the optimal, i.e. reconstructed shear modulus μ^{opt} are listed in Table 2 at each testing frequency. The results show that μ^{opt} is reasonably close to μ^{true} at all frequencies tested (with maximum relative error on the order of 1%), despite the changing environment in terms of material heterogeneity (outside Ω) and plane-wave excitation as described in Table 1. To test the sensitivity of the proposed scheme to measurement uncertainties, a 5% uniformly-distributed random noise was added to the synthetic observation data $\boldsymbol{u}^{\mathrm{obs}}$ in (4). The optimization results thus obtained are listed in the last column of Table 2 under label "$\mu^{\mathrm{opt}}_{\mathrm{noise}}$". At excitation frequencies equaling 100, 150, and 200 Hz, the reconstructed shear modulus is within 3% of its "true" counterpart, both in terms of its real and imaginary components. Only at 50 Hz, owing to the long wavelength of illuminating waves (relative to the measurement grid), the imaginary part of the shear modulus differs from the "true" value by 20%. In this case, the variation of the displacement field over the measurement region is diminished, which makes the reconstruction scheme more sensitive to input perturbations. However, even at this low frequency, the real part of the complex shear modulus is still close (3% relative error) to its "true" value. For clarity, the reconstruction results from Table 2 are plotted in Fig. 3 which indicates that the proposed methodology may provide an effective means for exposing the variation of the complex shear modulus with frequency, and thus enabling a comprehensive viscoelastic characterization of soft tissues.

6. Summary

In this study, an optimization-based scheme is proposed for the reconstruction of the "background" viscoelastic properties of a soft tissue from MR elastography measurements taken over a region where the tissue is predominantly homogeneous. To this end, the triaxial displacements observed over the featured (cubical) domain are split into (i) a *boundary subset* that is used to formulate a Dirichlet boundary value problem, and (ii) an *internal subset*, employed as an input to the minimization scheme. To aid the performance of the latter, material sensitivities of the featured cost functional are computed semi-analytically within the context of a BIE formulation, resulting in alternative "direct" and adjoint-field sensitivity formulas. The numerical results, obtained assuming geometric and material input parameters that are relevant to MR
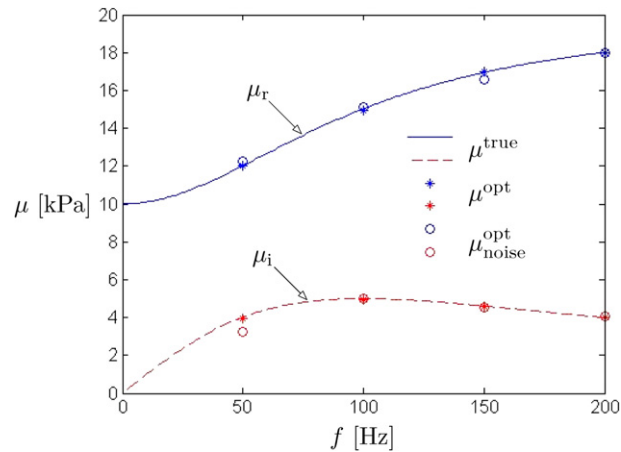
Fig. 3. "True" versus reconstructed values of the complex shear modulus versus frequency.

elastography, indicate that the proposed approach may provide an effective tool for comprehensive characterization of the "background" viscoelasticity of soft tissues.

References

[1] R. Muthupillai, P.J. Rossman, D.J. Lomas, J.F. Greenleaf, S.J. Riederer, R.L. Ehman, Magnetic resonance elastography by direct visualization of propagating acoustic strain waves, Science 269 (1995) 1854–1857.
[2] R. Muthupillai, P.J. Rossman, D.J. Lomas, J.F. Greenleaf, S.J. Riederer, R.L. Ehman, Magnetic resonance imaging of transverse acoustic strain waves, Magn. Reson. Med. (1996) 266–274.
[3] A. Manduca, T.E. Oliphant, M.A. Dresner, J.L. Manhowald, S.A. Kruse, E. Ameromin, J.P. Felmlee, J.F. Greenleaf, R.L. Ehman, Magnetic resonance elastography: non-invasive mapping of tissue elasticity, Medical Imaging Anal. (2001) 237–254.
[4] R. Sinkus, J. Lorenzen, D. Schrader, M. Lorenzen, M. Dargatz, D. Holz, High-resolution tensor MR elastography for breast tumour detection, Phys. Med. Biol. 45 (2000) 1649–1664.
[5] A.L. McKnight, J.L. Kugel, P.J. Rossman, A. Manduca, L.C. Hartmann, R.L. Ehman, MR elastography of breast cancer: preliminary results, Amer. J. Roentgenol. 178 (2002) 1411–1417.
[6] R. Sinkus, M. Tanter, T. Xydeas, S. Catheline, J. Bercoff, M. Fink, Viscoelastic shear properties of in vivo breast lesions measured by MR elastography, Magn. Reson. Imaging 23 (2005) 159–165.
[7] L. Huwart, F. Peeters, R. Sinkus, L. Annet, N. Salameh, L.C. ter Beek, Y. Horsmans, B.E. Van Beers, Liver fibrosis: non-invasive assessment with MR elastography, NMR Biomed. 19 (2006) 173–179.
[8] S.K. Venkatesh, M. Yin, J.F. Glockner, N. Takahashi, P.A. Araoz, J.A. Talwalkar, R.L. Ehman, MR elastography of liver tumors: preliminary results, Amer. J. Roentgenol. 190 (2008) 1534–1540.
[9] M.A. Green, L.E. Bilston, R. Sinkus, In vivo brain viscoelastic properties measured by magnetic resonance elastography, NMR Biomed. 21 (2008) 755–764.
[10] B.B. Guzina, M. Bonnet, Topological derivative for the inverse scattering of elastic waves, Quart. J. Mech. Appl. Math. 57 (2004) 161–179.
[11] M. Bonnet, B.B. Guzina, Topological derivative for the inverse scattering of elastic waves, Int. J. Num. Meth. Eng. 57 (2004) 161–179.
[12] M. Bonnet, Topological sensitivity for 3D elastodynamics and acoustic inverse scattering in the time domain, Comp. Meth. Appl. Mech. Eng. 195 (2006) 5239–5254.
[13] B.B. Guzina, H. Yuan, On the small-defect perturbation and sampling of heterogeneous solids, Acta Mechanica 205 (2009) 51–75.
[14] B.B. Guzina, I. Chikichev, From imaging to material identification: a generalized concept of topological sensitivity, J. Mech. Phys. Solids 55 (2007) 245–279.
[15] I. Chikichev, B.B. Guzina, Generalized topological derivative for the Navier equation and inverse scattering in the time domain, Comp. Meth. Appl. Mech. Eng. 197 (2007) 4467–4484.
[16] M. Bonnet, B.B. Guzina, Elastic-wave identification of penetrable obstacles using shape-material sensitivity framework, J. Comput. Phys. 228 (2009) 294–311.
[17] W.N. Findley, J.S. Lai, K. Onaran, Creep and Relaxation of Nonlinear Viscoelastic Materials, Dover, New York, 1989.
[18] J. Nocedal, S.J. Wright, Numerical Optimization, Springer, New York, 1999.
[19] M. Bonnet, Boundary Integral Equation Methods for Solids and Fluids, John Wiley & Sons, 1999.
[20] R.Y.S. Pak, B.B. Guzina, Seismic soil–structure interaction analysis by direct boundary element methods, Int. J. Solids Struct. 36 (1999) 4743–4766.
[21] T. Pritz, The Poisson's loss factor of solid viscoelastic materials, J. Sound Vib. 306 (2007) 790–802.
[22] J.J. More, D.J. Thuente, Line search algorithms with guaranteed sufficient decrease, ACM Trans. Math. Software 20 (1994) 294–308.